Topological Matter: A Unified Perspective on Real and Momentum Space

Simon Vecchioni,[1] Paritosh Singh,[2] Arpan De,[2] Miguel Chapa,[3] Vidya Singh,[1] Karol Woloszyn,[1] Ran Liu,[3] Bo Liu,[3] Chu-fan Yang,[1] Yoel P. Ohayon,[1] Ruojie Sha,[1] James W. Canary,[1] Joshua Hihath,[3] M.P. Anantram,[2] and Antia S. Botana[4]

[1] *Department of Chemistry, New York University, New York, NY 10003, USA*
[2] *Department of Electrical and Computer Engineering, University of Washington, Seattle, WA 98195, USA*
[3] *Center for Bioelectronics and Biosensors, School of Electrical Computer and Energy Engineering, Arizona State University, Tempe, AZ 85287*
[4] *Department of Physics, Arizona State University, Tempe, AZ 85287, USA*

(Dated: June 3, 2025)

Topology has emerged as a field for describing and controlling order and matter, and thereby the physical properties of materials. There are several largely disparate fields focused on examining and manipulating topology. One of these arenas is in the realm of real space, manipulating systems in terms of their spatial properties, to control the corresponding structural, mechanical, and self-assembling responses. Much of the work in soft matter topology falls within this domain. A second arena is in the domain of momentum or k-space wherein topology controls the features of the electronic band structure of materials, and topologically non-trivial features result in the development of materials with truly unique properties. This work focuses squarely on the realm of condensed matter physics. Here, we review concepts of real- and k-space topology and propose areas for convergence between these two disparate fields.

I. INTRODUCTION

When topological materials are mentioned, topological insulators are often at the forefront of the discussion [1–9]. Topological insulators represent a class of topologically non-trivial materials that are insulating in the bulk but electrically conductive at the interface with a conventional topological material (e.g. vacuum) [1]. Even though in recent years topology has acquired more and more importance in hard condensed matter systems, it also plays a central role in soft, non-crystalline materials. The behavior of many soft materials relies on vector fields, such as the nematic director in liquid crystals, velocity in fluids[10] or in active particles [11, 12], deformation in soft solids[13], or the orientation of fibers [14, 15]. All these fields can host singularities, or topological defects, which are crucial in determining the properties and behavior of soft systems [14, 16–18]. In fact, one can think of soft analogs of topological insulators as provided by topological mechanical networks, or phononic metamaterials, where the propagation of mechanical deformations is suppressed in the bulk material but allowed at the boundaries, thus creating edge modes similar to those found in topological insulators[19]. Further, topology is known to deeply affect the physical and biological properties of DNA [20] and to impact fundamental cellular processes [15, 17]. In this context, we review here how topology is inherent to this broad set of typically disparate disciplines with the ultimate goal of understanding how different fields could crosstalk and interact.

II. GENERAL CONCEPTS

Topology and geometry. Topology is a branch of mathematics sometimes referred to as "rubber sheet geometry," in which two objects are considered equivalent if they can be continuously deformed into one another through bending, twisting, stretching, or shrinking while disallowing tearing apart or gluing together parts. The main topics of interest in topology are the properties that remain unchanged by such continuous deformations. While similar to geometry, topology differs from it in that geometrically equivalent objects often share numerically measured quantities, such as lengths or angles, while topologically equivalent objects resemble each other in a more qualitative sense.

In many cases, the objects considered in topology are ordinary ones residing in three- (or lower-) dimensional space. For example, a simple loop in a plane and the boundary edge of a square in a plane are topologically equivalent, as may be observed by imagining the loop as a rubber band that can be stretched to fit tightly around the square. Each of these shapes can be defined by a single number, the "topological invariant" which is the same in both cases. On the other hand, the surface of a sphere is not topologically equivalent to a torus or the surface of a solid doughnut ring. Each of these shapes has a different topological invariant, and one can not be transformed into the other without modifying the invariant (Fig. 1). With this unpretentious picture in mind, we will start with simple geometrical definitions of topological invariants.

An intuitive example of global geometry and topology: Gauss-Bonnet. You may have heard a topologist described as "a mathematican who can't tell the difference between a donut and a coffee cup." As an example of the connections between geometry and topology, we start by discussing

https://doi.org/10.26434/chemrxiv-2025-swzkq **ORCID:** https://orcid.org/0000-0001-8243-650X Content not peer-reviewed by ChemRxiv. **License:** CC BY-NC-ND 4.0

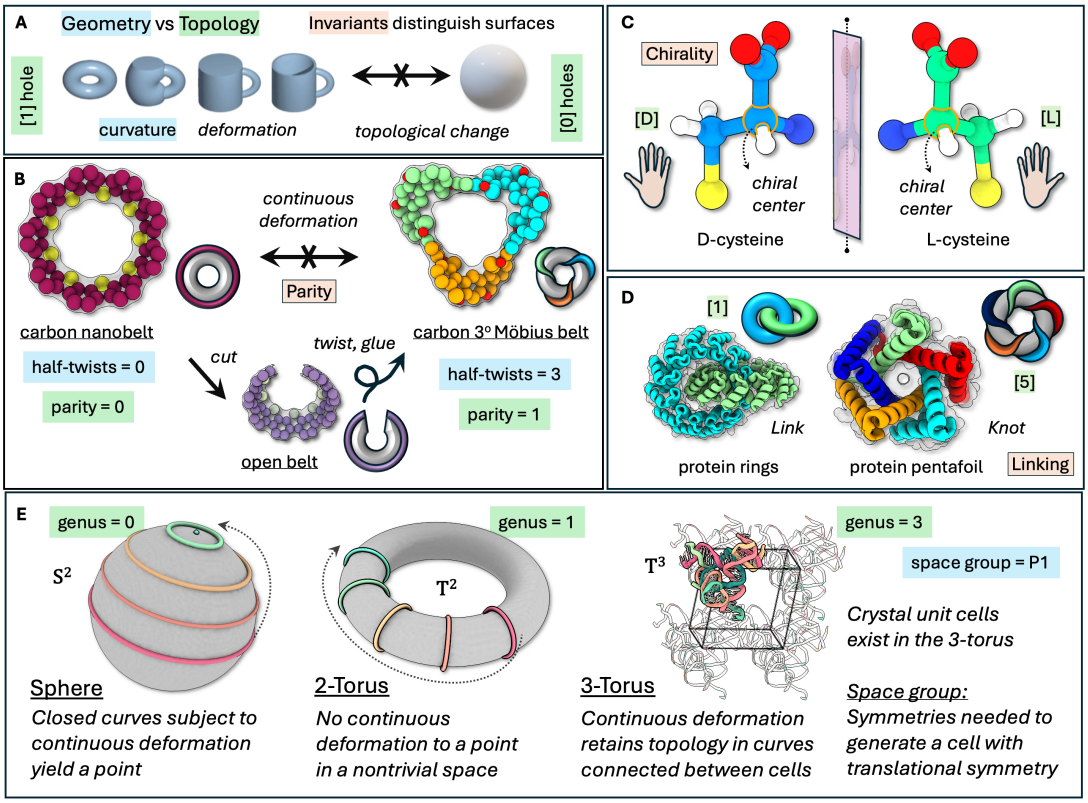


FIG. 1. Topology and geometry. (A) When we think of topology, we normally think of objects that cannot be simply transformed into each other: a rubber band and a Mobius strip are topologically different, a donut and a coffee mug are topologically equivalent. Topological invariants are shown in green, and geometric ones in blue. (B) A carbon nanobelt [21] and triply twisted Mobius belt[22] are shown. With an odd parity, or number of half-twists, the Mobius belt has a non-orientable surface and is topologically distinct from a simple nanobelt. Sulfur atoms are colored yellow and oxygen red, with carbons colored to show topology. Side chains are excluded for clarity. (C) Chiral molecules cannot be deformed into one another, yielding chiral building blocks that form the basis of living systems. (D) Protein rings [23] and pentafoil knots [24] have linking numbers 1 and 5, respectively, and cannot be unlinked without breaking chemical bonds. (E) Continuous deformation of closed loops on the sphere yields a point, while curves connected through the torus remain nontrivial. Crystal unit cells exist in the 3-torus, where the space group governs the symemtries needed to generate a translational unit cell in the torus.

an integral that will help us classify two-dimensional (2D) compact manifolds (surfaces without boundaries) embedded smoothly in three dimensions. This integral is "topologically invariant" in that if one such surface can be smoothly deformed into another, then the two will have the same value of the integral. The integral cannot tell the difference between the surface of a coffee cup and that of a donut, but it can tell that the surface of a donut (a torus) is different from a sphere. Such global integrals of geometrical quantities are a common origin of topological quantities in physics.

We start by considering a two-dimensional surface. At any point on the surface, there are two radii of curvature. We define the signed "Gaussian curvature" as $\kappa=(r_1 r_2)^{-1}$. We subsequently consider closed surfaces such as the sphere and the torus. The area integral of the curvature over the whole surface is "quantized", and is a topological invariant as shown by the Gauss-Bonnet theorem [25].

$$\int_M \kappa dA = 2\pi\chi = 2\pi(2-2g) \tag{1}$$

where g is the genus g=0 for a sphere, g= 1 for a torus and g= n for an n-holed torus. As we will see below, this is directly related to topological invariants in condensed matter.

Knot theory and linking number. Another area which is commonly encountered when exploring topology is knot theory. A knot is a closed curve which is topologically distinct from the unknot (a circle), and cannot be deformed into a simple loop. Knots can be distinguished from one another by a variety of invariants (Fig. 1). In order to perform a rigorous analysis of realspace knots, it is useful to look at knot diagrams, which are 2D projections of knots onto a surface. To distinguish knot diagrams, Kurt Reidemeister proposed three deformations that can reshape a given knot diagram for analysis. These three moves, known as twist, poke and slide operations, can be

https://doi.org/10.26434/chemrxiv-2025-swzkq ORCID: https://orcid.org/0000-0001-8243-650X Content not peer-reviewed by ChemRxiv. License: CC BY-NC-ND 4.0

performed, after which any number of invariants can be computed to determine the similarity or distinctness of given examples [26, 27]. Such invariants are often denoted as "colorations" and critical to classify, distinguish, and show equivalence between knot diagrams [28].

The most basic topological invariant of knots is the linking number, which describes the entanglement of two non-intersecting curves. When these curves are closed (e.g. circles, not lines), the linking number will always be an integer. A knot, in the traditional sense, is typically formed from a closed piece of string or rope, on which two parallel curves can be drawn on opposite sides of the material to compute the linking number. A formalism for computing the linking number was famously described by Gauss by defining topological invariant link (Lk) as the sum of geometric invariants twist (Tw) and writhe (Wr), and can be computed by evaluating the Gauss linking integral across these two curves [29]. Twist may be considered a form of curvature that follows the tangent vector, like a helix twisting about a central axis; while writhe can be considered curvature in the normal vector direction, or bending out of plane like DNA wrapping a histone.

The Gauss linking integral can be computed in the following way for non-intersecting, smooth curves K, L in realspace, parameterized by vector-valued functions $k(u), l(v)$:

$$\mathrm{Lk}(K,L) = \frac{1}{4\pi}\iint_{K\times L}\frac{\mathbf{k}-\boldsymbol{\ell}}{|\mathbf{k}-\boldsymbol{\ell}|^3}\cdot(d\mathbf{k}\times d\boldsymbol{\ell}). \qquad (2)$$

When K and L are each closed curves, $Lk(K,L)$ is integer valued [20]. Extensions of this continuous model have been made to study piecewise linear curves, or those composed of atoms and bonds in soft matter. Such an analysis generates a discrete linking integral of similar form, which generates integer-valued linking numbers for closed curves, and is useful in the analysis of real-space materials, as we will show below [30].

Periodicity, a key linkage between soft and hard (condensed) matter. Periodicity is a common concept that links topology in (hard) condensed and soft matter. As a direct analogy to momentum space, which is carried out in crystalline solids, one may define the unit cell of a real-space crystal–macromolecular, ionic, or otherwise–as being composed of repeated units subject to the same symmetries and groups as electron bands. A fundamental attribute of periodic systems is that they possess translational symmetry in each dimension. All atoms in the unit cell repeat under translation along integer copies of the fundamental lattice vectors (a, b and c). As a result of this requirement, realspace atoms inside periodic systems can be mapped to the 3-torus, or T^3. Any curve which exits one side of the unit cell must necessarily enter the opposing one, similar to traversing the inside of a 2-torus, or donut, where integer numbers of circumferences cause the walker to return to the starting point.

The torus is a fundamentally non-trivial space, possessing a hole along each lattice vector. A way to visualize this is shown in Fig. 1, where the 2-sphere (S^2) and 2-torus (T^2) are shown with closed curves on their surface. The continuous deformation of such loops on the sphere clearly degenerate to a point, while the holes of the torus protect the loops against such loss of information. Periodic systems thus map to an intrinsically non-trivial space that supports periodic entanglements and bands in both real and momentum space. In this manner, structures which are manifest in T^2 and commonplace throughout this review (not only in momentum, but also in real space).

To describe periodic systems, there are 230 different space groups defined which pervade crystallography and group theory. These space groups are matrix constructions that govern how the fundamental unit (or asymmetric unit in chemistry), is manipulated to form the unit cell. The glide, mirror and rotation operations of the space group are used to build the minimum object necessary to produce a cell in the 3-torus, which is a unit of space glued left-to-right, top-to-bottom, and forward-to-back, in a higher-dimensional version of the two-torus. Indeed, all periodic, 3D systems sit on the 3-torus (T^3), which is a topologically nontrivial space into which curves can become entangled, like threads in a textile, by this gluing. This crystal unit cell, a block of space in the 3-torus, is then subject to translational symmetry. In this way, the space groups themselves are geometric constructions within the topological space of the 3-torus. This is true for electron bands as well as for molecules in repeating lattices.

The periodicity in crystal materials in momentum space is represented by the Brillouin zone, or the momentum cell, and this is directly related to the crystal unit cell. This unit cell can be constructed empirically from the periodic nature of diffraction patterns in single crystals. Waves diffracting through a crystal, be they X-ray, electron or neutron, generate a conserved set of reflections that reflect the internal structure of the repeating unit. Such patterns form a 3D map in reciprocal space along a manifold known as the Ewald sphere, and is described by the relation:

$$\mathcal{S} = ha^* + kb^* + lc^* \qquad (3)$$

The surface of the Ewald sphere S has a radius of $1/\lambda$ around the origin, s_0 with unit cell vectors a,b, and c, inverse cell vectors of a^*, b^*, and c^* and h, k and l are integer constants.

The conditions for diffraction on such a surface hold under the application of Bragg's law:

$$n\lambda = 2dsin(\theta) \qquad (4)$$

where n is an integer, θ is the incident angle of the incoming beam, and d is the displacement vector between symmetry-equivalent atoms in neighboring unit cells (a, b, c in realspace and h, k, l in reciprocal space. We can solve for reciprocal vector $1/d$ by asserting the Ewald surface:

$$|\mathcal{S}| = 2sin(\theta)/\lambda = 1/d_{hkl} \qquad (5)$$

https://doi.org/10.26434/chemrxiv-2025-swzkq **ORCID:** https://orcid.org/0000-0001-8243-650X Content not peer-reviewed by ChemRxiv. **License:** CC BY-NC-ND 4.0

The Ewald sphere has been recently shown to be a complex, often irregular surface that is rarely an actual sphere [31]. The Ewald sphere of diffracting crystals and the Brillouin zone of conductive materials are analogous constructions. This intimate relation between waves passing through periodic units of different natures underscores the deep connection between realspace and momentum space phenomena; and by extension, often the realspace programming of crystalline materials will have profound effects on waves and bands that pervade k-space.

III. TOPOLOGY IN CONDENSED MATTER: K-SPACE

1. *Quantum Hall state and topological insulators*

The aforementioned Gauss-Bonnet example will form our basis for understanding the celeb invariants in condensed matter physics such as those in the integer quantum Hall effect [32] and topological insulators [1]. We will first need to incorporate one fact about solids: the Bloch theorem. This theorem exploits the translational symmetry/periodicity of the crystal to classify electronic states in terms of their crystal momentum $\mathbf{k}$ as defined in a periodic Brillouin zone. The Bloch states $|u_m(\mathbf{k})\rangle$ are eigenstates of the Bloch Hamiltonian $\mathcal{H}(\mathbf{k})$. The corresponding eigenvalues $E_m(\mathbf{k})$ define the energy bands.

Let's start then with the invariant used to describe the integer quantum Hall effect [33] in a 2D crystal (the first Chern number, also known as TKNN invariant [32]), as it follows from an integral of a related curvature to that of Gauss-Bonnet. Recall that the Gauss and Bonnet theorem states that the integral of the Gaussian curvature over a closed surface is a quantized topological invariant whose value is related to the genus g (which counts the number of holes). This enables us to topologically classify 2D surfaces by g. Now, instead of maps from two to three dimensions (which describe surfaces), we consider a 2D band structure that consists of a mapping from the crystal momentum (defined on a torus) to the Bloch Hamiltonian. When $\mathbf{k}$ is transported around a closed loop, $|u_m(\mathbf{k})>$ acquires a well defined phase called the Berry phase $\mathcal{A}_m =< u_m|i\nabla_k|u_m >$ [34], which may be expressed as the surface integral of the Berry flux $\mathcal{F}_m = \nabla \times \mathcal{A}_m$. The Chern invariant corresponds to the total Berry flux in the Brillouin zone.

$$n_m = \frac{1}{2\pi}\int d^2\mathbf{k}\mathcal{F}_m, \tag{6}$$

where n_m is an integer (quantized). The total Chern number is obtained by summing over all occupied bands:

$$n = \sum_{m=1}^{N} n_m \tag{7}$$

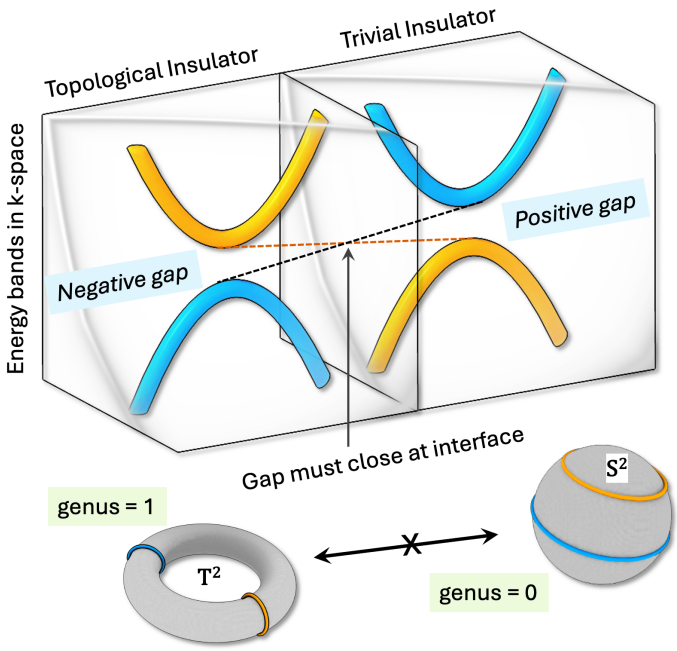


FIG. 2. The metallic surface of a topological insulator is different from an ordinary surface because its metallic nature is protected by certain symmetry invariants. In this sense, it cannot be simply transformed into the surface of a normal insulator. The sketches show the electronic structure for a "trivial" insulator (right) and a topological insulator (left). In both cases, there are allowed electron states (black lines) introduced by the surface that lie in the bulk band gap (the bulk valence and conduction bands are indicated by the green and blue lines, respectively). In the trivial case, even a small perturbation (say, changing the chemistry of the surface) can open a gap in the surface states, but in the nontrivial case, the conducting surface states are protected. Note that in the topological insulator, the surface states are linear in momentum space.

This is the first Chern number, also known as TKNN invariant as it was introduced by Thouless, Kohmoto, Nightingale and den Nijs [32]. The Chern number n is a topological invariant as it cannot change when the Hamiltonian varies smoothly. TKNN showed that this corresponds to the integer in the quantized Hall conductivity $\sigma_{xy} = n\frac{e^2}{h}$. The state responsible for the quantum Hall effect does not break any symmetries, but it defines a topological phase in the sense that certain fundamental properties (such as the quantized value of the Hall conductance, and the number of gapless boundary modes) are insensitive to smooth changes in materials parameters and cannot change unless the system passes through a quantum phase transition. The work of TKNN ultimately explains that the difference between a quantum Hall state and an ordinary insulator is a matter of topology, and this helped explain the robust quantization of σ_{xy}. In this manner, the study of the quantum Hall effect led to the classification paradigm based on the notion of topological order. As a simple example, imagine now an

https://doi.org/10.26434/chemrxiv-2025-swzkq **ORCID:** https://orcid.org/0000-0001-8243-650X Content not peer-reviewed by ChemRxiv. **License:** CC BY-NC-ND 4.0

interface where a crystal slowly interpolates as a function of distance between a quantum Hall state ($n = 1$) and a trivial insulator ($n = 0$). Somewhere along the way the energy gap has to vanish, because otherwise it is impossible for the topological invariant to change. Since the Hall conductivity (and hence the TKNN invariant) is odd under time reversal [35], the topologically nontrivial states described above can only occur when time reversal symmetry is broken either by an external magnetic field or by magnetic order.

The spin-orbit interaction allows a different topological class of insulating band structures when time-reversal symmetry is unbroken. The possibility of a time-reversal invariant 2D topological insulator was first noticed in a model of graphene with spin-orbit interactions (a so-called quantum spin Hall insulator) [36]. The fact that the edge states of the quantum spin Hall insulator are robust suggests that there must be a topological distinction between the quantum spin Hall insulator and an ordinary insulator. Using the bulk-boundary correspondence, which simply states that the invariant of the bulk dictates what occurs at the boundaries, it was shown that there are two and only two topological classes of time reversal invariant band structures as defined by the $\mathbb{Z}_2$[37] invariant ν, and that sets the stage of 2D topological insulators [6]. A 3D topological insulator is characterized by four $\mathbb{Z}_2$ topological invariants (ν_0, ν_1, ν_2, ν_3) [8, 9]. A topological insulator, like an ordinary insulator, has a bulk energy gap separating the highest occupied electronic band from the lowest empty band. The surface (or edge in two dimensions) of a topological insulator, however, necessarily has gapless states that are protected by time reversal symmetry (Fig. 2). In this manner, a topological insulator is closely related to the 2D integer quantum Hall state, which also has unique edge states. The surface (or edge) states of a topological insulator lead to a conducting state with properties unlike any other known 1D or 2D electronic systems [1]. In addition to their fundamental interest, these states are predicted to have special properties that could be useful for applications ranging from spintronics to quantum computation.

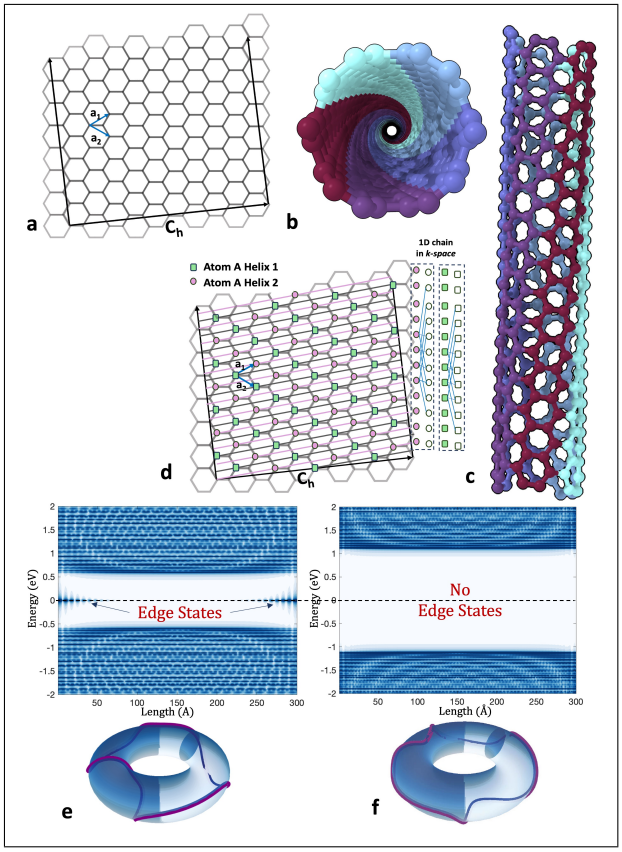


FIG. 3. (a) Structure of a chiral (6,4) carbon nanotube (CNT) showing the chiral vector $\mathbf{C_h}$ and graphene unit vectors $\mathbf{a}_1$ and $\mathbf{a}_2$. (b, c) Cross-sectional and lateral views of the CNT, respectively. (d) Mapping of lattice points from real space to momentum space along the circumferential direction, forming two helical one-dimensional chains corresponding to angular momentum channels $\mu = 0$ (pink) and $\mu = 1$ (green), which span the full length of the CNT. (e) *Top:* Density of states (DOS) for $\mu = 1$, showing two edge states within the band gap of the (6,4) CNT. *Bottom:* Phase plot of the Bloch function f_μ on a torus defined by momentum k and phase $\arg(f_\mu)$, showing clear winding along both meridional and longitudinal directions of the torus, resulting in a net winding number of 1. (f) *Top:* DOS for $\mu = 0$, showing no edge states in the band gap. *Bottom:* Phase plot of f_μ on the same torus, showing no winding along the meridional direction, resulting in a net winding number of 0.

2. *Topology in 1D systems: Carbon Nanotubes*

Carbon nanotubes (CNTs) are quasi-one-dimensional structures consisting of single-layer carbon atoms arranged in a hexagonal lattice forming cylindrical shells. These hollow tubes are classified by indices (n, m), which define their circumference as mapped onto a vector $\mathbf{C_h} = n\mathbf{a}_1 + m\mathbf{a}_2$ in the underlying planar graphene sheet (Fig. 3). Here, $\mathbf{a}_1$ and $\mathbf{a}_2$ are the primitive lattice vectors of graphene. CNTs have attracted significant attention in engineering applications due to their unique electronic properties. Depending on the indices (n, m), CNTs can exhibit either metallic or semiconducting behavior, making them promising candidates for various electronic applications such as interconnects and transistor channels [38].

Given their quasi-one-dimensional nature, a fundamental question arises regarding the relationship between their band structure and edge states. Research since the 1990s has confirmed this relationship [39]. In 2019, Okuyama, Izumida, and Eto established that topologically protected edge states exist in all semiconducting CNTs where $n \neq m + 1$ [39]. This finding is particularly significant because these edge states can withstand various interactions, including those with other nanotubes, defects, and substrates, making them robust in experimental settings despite the inherent flexibility of nanotubes.

https://doi.org/10.26434/chemrxiv-2025-swzkq **ORCID:** https://orcid.org/0000-0001-8243-650X Content not peer-reviewed by ChemRxiv. **License:** CC BY-NC-ND 4.0

Okuyama *et al.* also demonstrated that a nanotube of any chirality (n, m) can be topologically mapped to a set of purely one-dimensional helices spanning the entire length of an infinitely long carbon nanotube. Consequently, the carbon nanotube Hamiltonian can be represented by purely one-dimensional Hamiltonians in mode space, where each mode corresponds to a specific angular momentum. The exact number of these 1D Hamiltonians depends on the indices (n, m) (see an example in Fig. 3).

By analyzing the band structure of these simplified 1D Hamiltonians and calculating the topological invariance, they established that there are $4(n-m+1)/3$ edge states for a semiconducting CNT. In a perfectly periodic CNT (without defects, bending, or twisting, and with minimal circumference termination at both edges), all $4(n-m+1)/3$ edge states exist at the middle of the bandgap. Under perturbation, while the number of edge states remains invariant due to topological protection, their energies may deviate from the midgap position [40] (Fig. 3). This observation shows that the presence of chiral symmetry in real space of CNT leads to the topologically protected energy edge states in momentum space (*k-space*).

IV. TOPOLOGY IN PERIODIC SOFT MATTER

As mentioned above, the most basic topological invariant of knots is the linking number, which describes the entanglement of two non-intersecting curves. When these curves are closed (e.g. circles, not lines), the linking number will always be an integer. Most macromolecular crystals do not explicitly present topological features, as the atoms in adjacent cells rarely link in the band-like structures that appear in momentum space. Before describing discoveries in this space, we first note two mathematical constructions of polymeric molecules. A typical polymer can be considered a discrete, piecewise continuous (non-smooth) curve in real-space ($\mathbb{R}^3$) that does not form a closed loop [41]. Topological constructions of open polymers are fundamentally unknotted, and such a description is typically not useful in classifying different macromolecules. We thus invoke a a class of knot-like structures, known as "knotoids," which are entanglements with two ends on a single open curve [42]. An extension lies in the "linkoid," which is an entanglement of more than one open curve, each possessing two end points, and extremely relevant to polymeric macromolecules [43] . This is the same type of structure that is formed by tying shoelaces–though it is not a knot *per se*, so long as the ends are not pulled through a crossing, the structure is held invariant and functional. In much the same way, polymeric structures can be described as topologically non-trivial by an analysis of their structure without passing ends over crossings.

In Fig. 4 we show two DNA constructs that form periodic linkoids. Based on the underlying rotation of the helices prescribed by the number of base pairs between junctions, two realspace topologies can be obtained: one right-handed and one left-handed embedded ring with opposite crossing signs at the junctions [44]. In this system, the invariants are the linking number (+3 in both cases), as well as the crossing signs (+ and - for RH and LH, respectively). Both structures assemble into periodic crystals that diffract X-rays, yielding Friedel pairs that can be mapped to the Ewald surface in HKL.

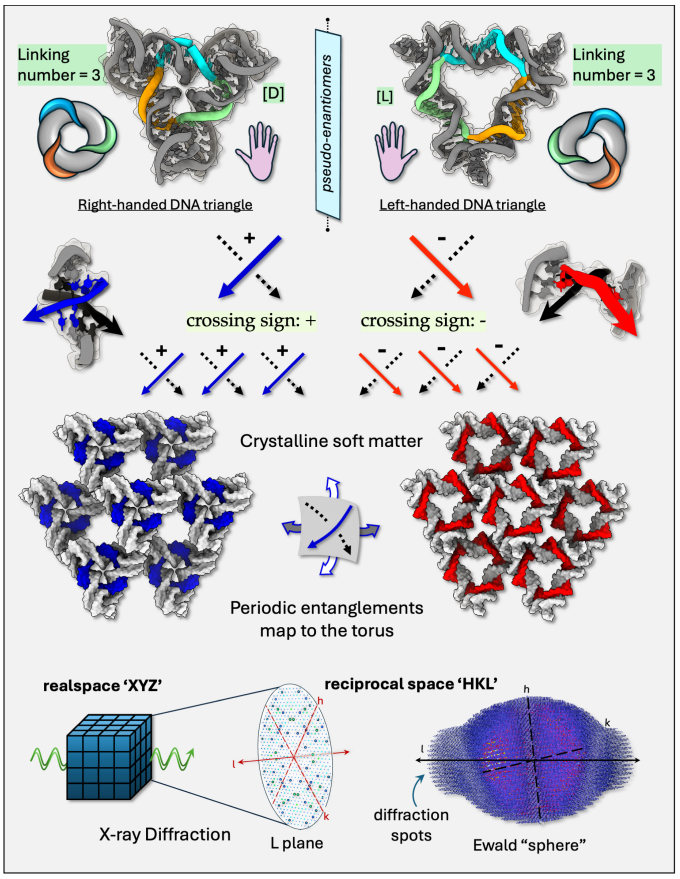


FIG. 4. Construction of periodic structures from topological real-space components. Two DNA triangle tiles are shown [44] which exhibit left- and right-handed topologies as a result of the helical twist, a geometric invariant. Both have a linking number of 3 about the center (rainbow) strand. One possesses a positive (blue) crossing, and the other a negative (red) crossing. These tiles self-assemble into periodic 3D crystals. A mapping of curves to the 2-sphere is shown, where continuous deformation of a closed curves yields a point. By contrast, closed curves on the 2-torus cannot be deformed to a point, as with real-space macromolecules embedded in the 3-torus, the basis of crystal tiling. Single crystals diffract x-rays, yielding diffraction patterns in the reciprocal plane, HKL. Real diffraction data are shown.

https://doi.org/10.26434/chemrxiv-2025-swzkq **ORCID:** https://orcid.org/0000-0001-8243-650X Content not peer-reviewed by ChemRxiv. **License:** CC BY-NC-ND 4.0

V. TOPOLOGICAL MATERIALS IN REALSPACE SOFT MATTER

1. *Textiles*

The earliest uses of topological materials by humans stem from forming knots in rope and fabrics. Textiles represent a rich set of periodic knots in two dimensions, and are the most ubiquitous form of artificial link available. Much work has been done to characterize knots in the plane [45], and by extension periodic knots that form everyday fabrics (Fig. 5A) [46, 47]. An important feature of 2D periodic structures with translational symmetry is that they map to the 2-torus ($T^2 = S^1 \times S^1$). This means that curves that exit the left side of the plane graph will enter diametrically opposed on the right side, and same with the top and bottom (Fig. 5A). This is intuitively related to early side-scrolling video games where a player exits stage left and appears on the other side of the screen. As can be seen in Fig. 1, a sphere is a topologically trivial space in which a closed curve can be deformed into a point. By contrast, closed curves embedded into the torus–under the criterion that such closed curves are not trivially contained within a single cell–will generate complex topological features across their lattices. The use of toroidal embeddings of knotoids and linkoids into periodic fabric is the means by which humans have spun, woven and knitted clothing from plant and animal fibers, with evidence going back as far as 30,000 years [48].

Various invariants have been proposed to distinguish textile links, including the crossing number (a geometric invariant that describes the total number of over- and under-passes), the linking number, and the Jones polynomial, which breaks a knot diagram into a series of crossings that can be analyzed computationally [49–51]. Using a series of repeating links, recent work has been carried out to form chain-mail like structures in 3D, forming so-called polycatenated architected materials (PAMs)(Fig. 5A) [52]. These structures are periodic tangles that have the structural properties of both dense foams and tear-resistant fabrics, exhibiting non-Newtonian fluid dynamics with both the ability to resist stretching and compression [53]. Indeed the relationship between periodic polymer entanglement and mechanical properties has been established from both an experimental and topological perspective [54].

2. *DNA*

Topology deeply affects the properties of DNA and impacts fundamental cellular processes, such as gene expression, genome replication, chromosome structure and segregation [55]. In all organisms, DNA topology is carefully modulated and the supercoiling degree of defined genome regions may change according to physiological and environmental conditions. Indeed whole classes of enzymes are dedicated to the topological winding and unwinding of DNA (Fig. 5B). These enzymes are known as topoisomerases, and come in a variety of flavors to increase or decrease the supercoiling of DNA [56–58]. An additional class of enzymes, known as (junction) resolvases, make and break branches to drive genetic recombination during germ cell division, or meiosis, in eukaryotes [59].

DNA is described most aptly by the linking invariant, as well as the quantities twist and writhe. Indeed, the ability of this formalism to apply to nucleic acids led to an early union of knot theory in R^3 and DNA structure. This was first applied to DNA in 1971 with a mathematical description of the writhe number for a continuous, closed curve [20] to investigate supercoiling. The success of this analysis led to the interest and development of synthetic knots and linkoids from DNA.

The field of structural DNA nanotechnology was founded to exploit the programmability of DNA for topological self-assembly, or so-called "semantomorphic science." Founded in 1982 by Ned Seeman when he proposed the use of branched DNA motifs for the construction of periodic crystalline lattices [60], three special features of the DNA molecule made this a tractable approach: (1) based on Holliday junctions observed in meiotic recombination, an immobile branched junction was developed to enable architectures with complex topologies [61]; (2) A programmable base sequence allows for high-resolution design placement of topological features, the length, twist and writhe of duplex features, and the ability to add semantic tags that respond to chemical information; and (3) In the same way that restriction enzymes can recongnize and create complementary overhangs, the use of "sticky ends" between complementary tiles can generate 2D and 3D self-assembly by molecular recognition [62].

The first topologically-nontrivial synthetic DNA object was reported in 1991 [63] with the construction of six entangled catenanes with the connectivity of a cube (Fig. 4B). Since that time, branched junctions have been used to build both finite and extended arrays of DNA tiles, often with repeating tiles that exhibit crystalline symmetry. The double crossover was a pivotal motif that enabled the first extended 2D arrays, as well as providing the foundation for DNA origami [64]. 2D DNA arrays are akin to weaving and knotting, and analogies have been drawn between the possible DNA arrays and the vast collection of textiles scattered throughout the world's markets and art museums [65].

Complex 3D architectures have similarly been constructed, filling trigonal, tetragonal, hexahonal, rhombohedral and cubic space groups [86–89]. These architectures can be enzymatically or chemically ligated, yielding 3D architectures with periodic entanglements [69]. We have recently described the topological features of 3D DNA tiles which yield chiral tertiary structures, an emergent topological invariant of the branched supramolecular assembly. The geometric influence of twist, writhe and torsion play a strong role in determining the supramolecular chirality of DNA assemblies [44].

https://doi.org/10.26434/chemrxiv-2025-swzkq **ORCID:** https://orcid.org/0000-0001-8243-650X Content not peer-reviewed by ChemRxiv. **License:** CC BY-NC-ND 4.0

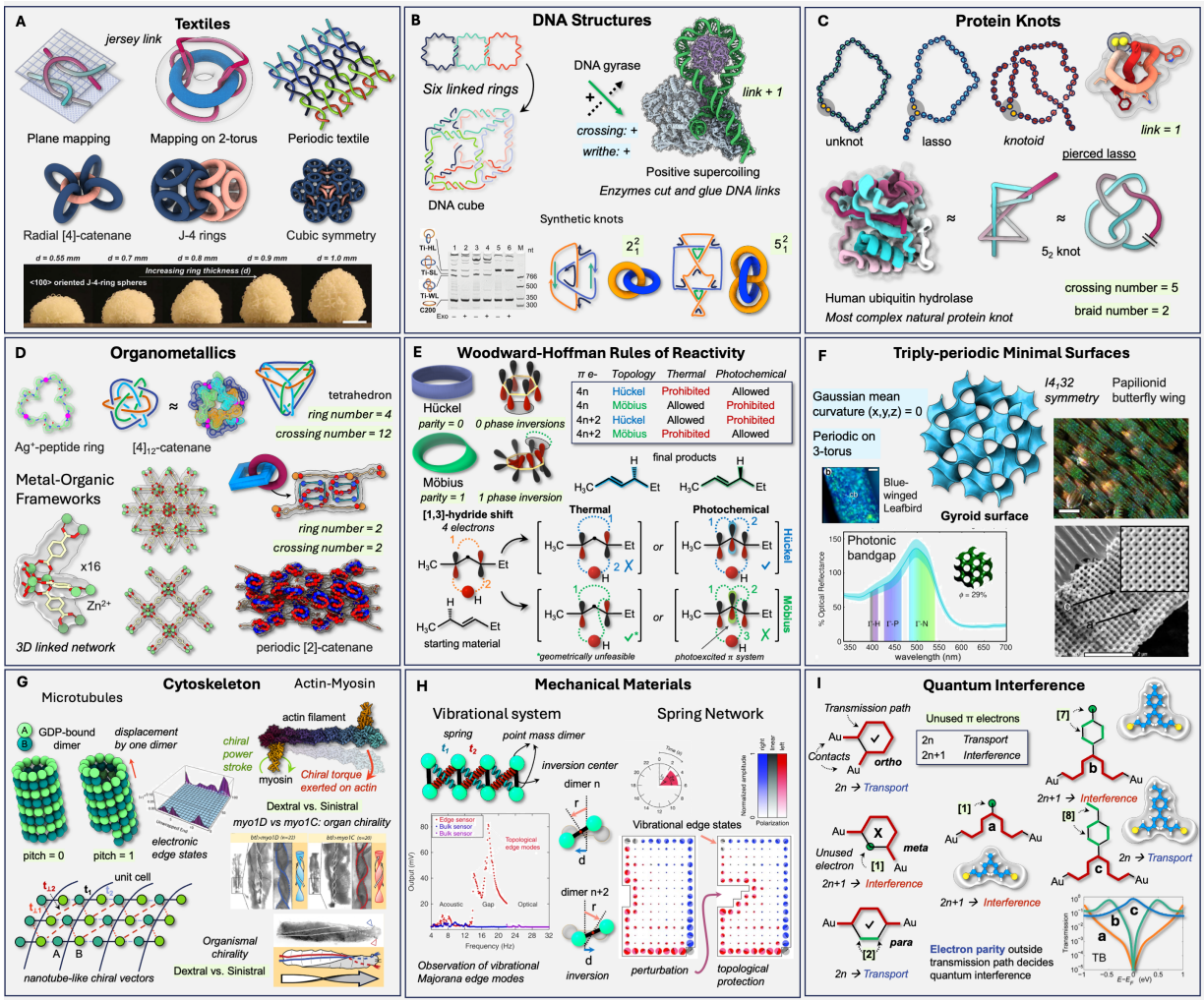


FIG. 5. Topology in synthetic and natural materials. (A) Textiles are made from periodic entanglements that can be mapped onto the 2-torus [51]. Polycatenated architected materials are 3D foam-like textiles made from entangled rings [52]. (B) DNA, as a primordial textile, can be fused into polycatenated species [60], [66] , and work has shown a class of enzymes which cut and twist DNA to affect its topology [58]. (C) Proteins are also made from open curves, but they benefit from closure by disulfide bonds. The most common form of linked protein is the pierced lasso [67, 68]. The highest order natural protein knot is the human ubiquitin hydrolase [69–71]. (D) Short peptides have been fused via metal coordination to make knotted finite objects [72], while periodic arrangements assemble into porous metal organic frameworks [70, 73, 74]. (E) Following the geometric strain and topological phase of pi electrons in reactions with a cyclic intermediate, the Woodward-Hoffman rules identify whether a reaction will happen based on the Mobius or Huckel topology of the ring [75]. (F) Triply-periodic minimal surfaces have zero Gauss curvature along three axis vectors and are embedded in the 3-torus. They arise naturally across biological systems and are used in photonic crystals [76, 77]. (G) In the cytoskeleton, responsible for cellular motion and division, microtubules can self assemble with nanotube-like chiral vectors and exhibit electronic edge states [78, 79]. Mysosin, a chiral molecular motor, can be engineered to be out of equilibrium and affect the hierarchical cihrality of whole organisms [80, 81]. (H) Using vibrating springs, groups have simulated electronic band strucutre in phonons to produce topological edge states [19, 82]. (I) In a similar way to chemical systems, tracking aromatic electrons in conjugated molecules dictates the conductance or interference in single molecule channels [83–85].

3. *Proteins*

Also composed of open curves of programmable length, polypeptides and proteins are ubiquitous manifestations of encoded polymer materials. Nearly all protein molecules are a form of knotoid, as they are formed from open polypeptides, and can thus be analyzed by twist, writhe, and crossing number. There has, however, been recent work establishing that protein molecules themselves can be formed in knotted topologies by gluing disulfide bonds to lock peptide chains into closed structures [67]. Haglund and colleagues have established the widespread existence of the “pierced lasso topology”, in which a disulfide bond creates a loop that is pierced by one or both endpoints,

https://doi.org/10.26434/chemrxiv-2025-swzkq ORCID: https://orcid.org/0000-0001-8243-650X Content not peer-reviewed by ChemRxiv. License: CC BY-NC-ND 4.0

in violation of Reidemeister move II, or the "poke" rule. It is estimated that nearly 18% of proteins in the Protein Databank with disulfide bonds have a complex pierced lasso topology. A database has been constructed for knotted proteins, with the most comlex example being Human ubiquitin hydrolase, which exhibits the topology of a 5_2 knotoid (Fig. 5C) [90, 91].

More recently, Panagiotou and colleagues have developed an open form of the linking integral that calculates the partial linking of periodic molecular chains [72]. Using this method they have shown that protein crystals can, in fact, possess non-trivial topologies relating to their overlapping strands and the symmetry of crystals after taking into account embedding into the 3-torus that describes crystal unit cells. These peptide chains are moderately entangled across the periodic crystal lattice, and cannot be unknotted without breaking the overall solid, similar to the electron bands in condensed matter. In fact, the polymer "bands" in macromolecular structures form a deeply connected analog of wave topology in momentum space.

4. *Organometallics*

Synthetic structures formed from peptide and organic precursors have been of interest for several decades for use in catalysis and electronics. Structures with organic (carbon) backbones and inorganic (metal) bridges can be formed into 1D catenantes or 3D networks known as metal-organic frameworks (MOFs). Synthetic metal-peptide rings, in which short peptide sequences are wrought into rings through the coordination of transition metals, have been characterized by their ring and crossing numbers. Topologically-nonequivalent frameworks have been constructed, depending on the amino acid sequence, including a T_2-tetrahedral link and a three-crossed tetrahedral link that are both mediated by Ag^+, composed ring numbers of 4 and crossing numbers of 12, and employ different tripeptide sequences (Fig 5D) [92].

MOFs are crystalline 3D extensions of organimetallic complexes, in which the coordination geometry of the metal and the symmetry and connectivity of the organic ligands establish the framework's hierarchical lattice and emergent functionality. This structural tunability underpins their potential in gas storage and separation, catalysis, drug delivery, and sensing [73, 93, 94]).

An early example of an interconnected, cubic MOF with large pores was presented in 1999 [74], mediated by repeating Zn^{2+}-bound units (Fig. 5D). Topological characterization of MOFs has largely been carried out on their symmetry groups [70], but there exist examples of MOFs with catenated repeats that are reminicent of PAM textiles [19]. Such catenated architectures may bridge the mechanical properties of textiles with the electronic properties of MOFs, enabling a foray into k-space topology by realspace molecular engineering.

5. *Woodward-Hoffman Rules of Chemical Reactivity*

In smaller molecular systems, topology plays a fundamental role in governing the reactivity, selectivity, and feasibility of organic reactions, particularly in pericyclic reactions. These reaction have a transition state follows a cyclic geometry and the bond orbitals (i.e. the electronic structure) are therefore subject to the topological rules of closed ribbons. These processes have been rationalized through the Woodward-Hoffmann rules, which predict the stereochemical outcomes of pericyclic reactions based on orbital symmetry consideration [83]. In general, for reactions involving $4n$ π-electrons (n = 1, 2, 3,...), thermally-induced suprafacial processes, in which the same faces of the π system are involved in the reaction, are symmetry forbidden and photochemically favored. By contrast, antarafacial pathways, in which the opposite faces of the π system are involved in the reaction, are symmetry allowed and photochemically disfavored. The opposite holds for systems involving $4n+2$ π-electrons. These selection rules can be further elucidated through the lens of the orbital topology of transition states: transition states adopting a Hückel topology have an even number of orbital phase transitions, whereas those following a Möbius topology have an odd number of orbital phase transitions (Fig. 5E). This additional consideration helps rationalize experimental observations. For instance, although a thermal [1,3] hydride shift is symmetry-allowed in an antarafacial manner according to the Woodward-Hoffmann rules, the required Möbius topology renders the transition state geometrically inaccessible. Consequently, such shifts are not observed under thermal conditions. This can further rationalize why enol isomerization requires an acid or base catalyst.

6. *Triply-Periodic Minimal Surfaces*

Leaving the nanoscale world of chemistry, we turn to biological systems, which harness geometric and topological structures at the microscale. The most pervasive type of geometric material in biological systems is the minimal surface, which exhibits zero Gauss curvature at all points. These materials are found everywhere in nature, from soap films to the inner membranes of the mitochondria–in each case minimizing an energy function, often a surface-area-to-volume problem. Of particular usefulness are materials that are both periodic and curvature-minimized, so-called triply-periodic minimal surfaces (TMPS). TMPS materials exhibit several morphologies, the most famous being the gyroid surface (Fig. 5F). With cubic lattice symmetry, but composed of a single, continuous surface, TMPS materials have been shown to exhibit superlative thermal, electrical and optical behaviors [76]. Indeed, many biological systems have leveraged TMPS architectures as photonic crystals–which interact with light using wavelength-matched periodic structures-including the iridescent patterns in butterfly wings and bird plumage

https://doi.org/10.26434/chemrxiv-2025-swzkq **ORCID:** https://orcid.org/0000-0001-8243-650X Content not peer-reviewed by ChemRxiv. **License:** CC BY-NC-ND 4.0

(Fig. 5F) [75, 77]. By changing the grain boundaries and lattice constants of such grown systems, organisms are able to construct complex coloration patterns with specific, tunable photonic features. In particular, it has been shown that the dynamic modulation of the refractive index in periodic guanine crystals generates the cloaking (photonic stopband) features famous in chameleons [95].

7. *Cytoskeleton.*

We next turn to the cytoskeleton, a collection of self-assembling tubes and fibers that govern cellular processes as diverse as division, locomotion and endocytosis (Fig. 5G). [96] Microtubules, helical cylinders made of tubulin dimers, are assembled and dissasembled in a non-equlibrium processes that has been exploited to generate work at the nanoscale in engineered systems [78, 97]. Recent studies have investigated the production of differing tube topologies, directly drawing on the chiral vectors of carbon nanotubes to show electronic band structure and edge states and ultraviolet superradiance (Fig. 5G)[79, 98].

Actin falls in another class of cytoskeletal fibers, and is coupled with motor protein myosin to carry out intracellular vesicle transport, exert forces on the cell surface, and actuate whole muscles [80, 99]. A recent study showed that the power stroke generated by protein myo1D was sufficient, when over- or under-expressed, to generate a chiral force that pertubed the chirality of fruit flies across scales, from the cell to the whole organism level (Fig. 5G, right) [80, 81]. In this way, a molecular motion subject to a topological quantity (left- and right-handedness) is able to affect the organization and geometry of living creatures in a hierarchical manner to twist whole organisms, underscoring the deeply impactful effect of single molecules and polymers on the material world.

8. *Mechanical Materials*

Powerful ideas from topologically non-trivial electronic systems have recently begun to be explored also in bosonic systems. Topologically protected acoustic, mechanical, and optical edge states have been demonstrated in a number of systems that recreate the requisite topological conditions. We focus here on vibrational materials that have been explored as a fascinating case of realspace, macroscopic materials that interact with waves in a periodic manner to produce topological effects akin to electron bands. Recent work using rigid bodies connected by springs of tunable constants have yielded particle-hole symmetry in the vibrational modes, yielding complex Majorana edge modes (Fig. 5H, left)[100]. These systems provide a means of tuning topological features by building macroscale waveguides. Other phononic metamaterials have been constructed to enable mechanical versions of the quantum spin Hall effect and the valley degree of freedom for unidirectional phononic signal guiding. Such findings demonstrate the potential of exotic topological phases in bosonic settings and should stimulate robust control and guiding of mechanical energy for signalling and filtering applications.

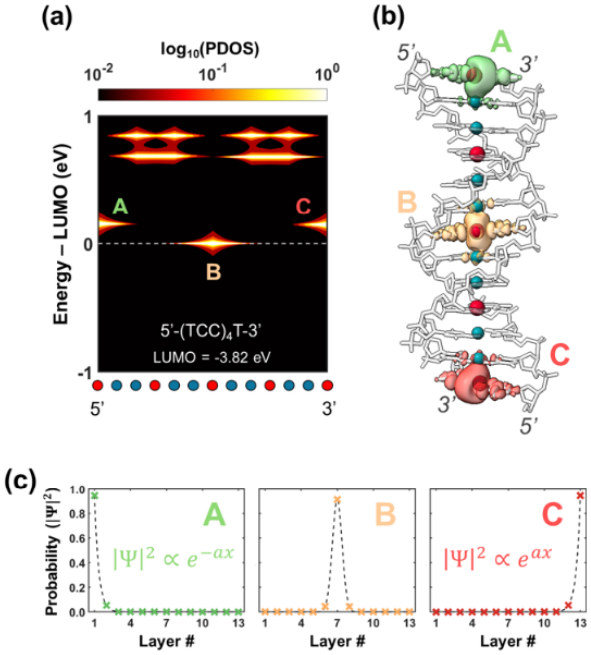


FIG. 6. Edge states in metallo-DNA nanowires. Computational demonstration of edge states in a finite 13-bp metallo-DNA motif comprising silver (Ag^{+}) and mercury (Hg^{2+}). We have used the sequence 5'-$(TCC)_4$T-3', where T and C represent (T:Hg^{2+}:T) and (C:Ag^{+}:C) metalated base pairs respectively. (a) Density of states for each metalated base pair within the energy window spanning from (LUMO-1eV) to (LUMO+1eV). Eigenstates A and C are identified to be the localized edge states while B corresponds to a bound state. The spatial locations of eigenstates A, B, and C are shown in (b) with wavefunction (Ψ) contours. The corresponding probability ($|\Psi|^2$) of finding electrons in these states are presented in (c), revealing the exponential characteristics of the edge states (A and C). In (a, b), the red and blue circles represent silver (Ag+) and mercury (Hg^{2+}) respectively. Notably, in (b), ($|\Psi| > 0.01$) are shown. The dotted black lines in (c) are obtained by curve fitting.

VI. CONVERGENCE BETWEEN REALSPACE MATERIALS AND RECIPROCAL SPACE TOPOLOGY

Having established the link between realspace topology–based on link, writhe, crossing, and periodic entanglements of various kinds–and the bands that govern waves in k-space, be they photons, electrons or phonons, we suggest a path forward in the rational design of the next-generation of topological materials. In particular, we emphasize that periodic systems in realspace, with their

https://doi.org/10.26434/chemrxiv-2025-swzkq ORCID: https://orcid.org/0000-0001-8243-650X Content not peer-reviewed by ChemRxiv. License: CC BY-NC-ND 4.0

tactile description and facile programming language, are a ripe medium for the engineering of band structure of these materials in momentum space. We have seen that carbon nanotubes have a realspace chiral vector that is simple to describe, but yields highly-nontrivial topological bands in momentum space (Fig. 3). The link between the two can be seen with the toroidal projection of the winding number in Fig 3, and the period of an atomic group A around the nanotube down the chiral vector is intrinsically linked to the winding of the Bloch phase in k-space, leading to edge states. Nanotubes are a good example of a hybrid material, but are not composable or readily accessible for re-engineering.

Soft-matter, molecular systems on the other hand, lend themselves more directly to engineering designs. Above we noted that real-space topology controlled the structure of the molecular orbitals, and thereby the selection rules for chemical reactions. However, these changes in orbitals also translate directly into the electronic charge transport properties in molecular electronic systems. There has been significant interest in recent years about how topological features in these structures relate to quantum interference (QI) in molecular devices [84, 85, 101–104]. Through these works, several graphical approaches that allow one to map specific molecular conjugation features to destructive or constructive quantum interference (DQI/CQI) in molecular systems (Fig. 5I)[84, 105, 106]. As a specific example, Stuyver et al.[107] directly studied how aromatic and antiaromatic bonding affects charge transport in extended porphyrin molecules in both Hückel and Möbius molecular configurations in different redox states (Fig. 5E) . In the Hückel systems, if the electrodes are attached through the extended axis of the porphyrin, aromatic structures (4n+2 π-electrons) display smoothly varying transmission probabilities across a wide range of energies, suggesting only CQI plays a role. In antiaromatic Hückel structures (4n π-electrons) sharp DQI transport features appear between the Highest Occupied and Lowest Unoccupied Molecular Orbitals (HOMO/LUMO), resulting in several orders of magnitude decrease in the predicted transport probabilities in the two cases.

Interestingly, the Möbius structures demonstrated DQI features in the transmission probabilities regardless of whether in their aromatic (4n π-electrons in this case) or antiaromatic (4n+2 π-electrons) states. Though these DQI features were typically not located within the HOMO-LUMO energy gap, and centered around other energy levels, thus decreasing the likelihood that the effects could be observed in experimental transport measurements. These results indicate that this topological change in realspace have profound effects on the molecular electronic structure and the charge transport properties of the systems, and that by simple reduction of the porphyrin (add 2 electrons), topological effects can be directly demonstrated in these systems.

Beyond the limits of CNTs and small molecules, DNA lends itself to a system that could be re-engineered in both realspace using techniques from DNA nanotechnology, and in k-space by controlling the electronic structure of the bases in the system. The DNA molecule has been extensively studied in realspace as a textile-like material that exhibits intrinsic twist, emergent writhe, and programmable link, and has been coaxed into periodic architectures. This platform is ripe for re-engineering, but lacks a strong interaction with waves, be they photonic, electronic or phononic. A recent work by Posnjak and colleagues has shown that lattice engineering in a periodic DNA structure at half-wavelength periods, and subsequent functionalization with titania, was able to yield photonic stopbands in the near-UV [108]. This proof-of-principle demonstration shows that a careful engineering of the material properties of DNA can yield nontrivial behavior in momentum space.

Metallo-DNA nanowires have emerged as a compelling platform for the development of ultra-scaled, highly-programmable, and cost-effective nanotechnologies, with large implications across nanoelectronic and nanophotonic domains. Our recent study (Fig. 6) elucidates the pivotal role of strongly-correlated metal ion chain embedded within a DNA framework. We observed that the metal ion chain plays a decisive role in modulating the charge transport properties of metallo-DNA nanowires, particularly within the energy regime of the lowest unoccupied molecular orbitals (LUMOs). The strategic placement of these metal atoms facilitates modulation of coupling between adjacent metalated base pairs – a feature that can be leveraged to realize one-dimensional topological insulators.

VII. CONCLUSION AND OUTLOOK

In this review, we have set out to frame the fundamental principles of curvature in real and momentum space, and to provide a unified perspective of topology for an audience of moderate technical know-how from various disciplines. We have surveyed a variety of materials in realspace, from textiles to phononic networks, and have made the case that realspace lattice engineering can generate a wide variety of phenomena in k-space. We anticipate that upcoming breakthroughs in materials design can be accelerated and guided by keeping the connections between disparate fields in mind. It is clear that biological and chemical systems are already deeply reliant on the connections between real and momentum space topology. And by providing a perspective on these relationships, we anticipate that convergent engineering with these principles will yield advances in topological quantum, electronic, phononic and photonic materials.

ACKNOWLEDGEMENTS

This work was funded by grant GCR-2317843 from the National Science Foundation to A.S.B., M.P.A., J.H., and J.W.C. We acknowledge support of grants N000141912596

https://doi.org/10.26434/chemrxiv-2025-swzkq **ORCID:** https://orcid.org/0000-0001-8243-650X Content not peer-reviewed by ChemRxiv. **License:** CC BY-NC-ND 4.0

from the Office of Naval Research, DE-SC0007991 from the Department of Energy, NASA Space Technology Graduate Research Opportunity 80NSSC24K1386, and a Ludo Frevel Crystallography Scholarship administered by the International Centre for Diffraction Data.

[1] M. Z. Hasan and C. L. Kane, Rev. Mod. Phys. **82**, 3045 (2010).
[2] A. Anirban, Nature Reviews Physics **5**, 267 (2023).
[3] J. Wang and S.-C. Zhang, Nature Materials **16**, 1062 (2017).
[4] J. E. Moore, Nature **464**, 194 (2010).
[5] M. G. Vergniory, L. Elcoro, C. Felser, N. Regnault, B. A. Bernevig, and Z. Wang, Nature **566**, 480 (2019).
[6] C. L. Kane and E. J. Mele, Phys. Rev. Lett. **95**, 226801 (2005).
[7] B. A. Bernevig, T. L. Hughes, and S.-C. Zhang, Science **314**, 1757 (2006), https://www.science.org/doi/pdf/10.1126/science.1133734.
[8] L. Fu and C. L. Kane, Phys. Rev. B **76**, 045302 (2007).
[9] J. E. Moore and L. Balents, Phys. Rev. B **75**, 121306 (2007).
[10] P. L. Boyland, A. Hassan, and M. Stremler, J. Fluid. Mech. **403**, 277 (2000).
[11] M. Y. Zion, Y. Caba, A. Modin, and P. M. Chaikin, Nat. Commun. **13**, 1 (2022).
[12] L. A. Komarov, N. P. Krychkov, and O. Yurichenko, Stanislav, Soft Matter **14**, 9657 (2018).
[13] S. Huang, G. Pessot, P. Cremer, R. Weeber, C. Holm, J. Nowak, S. Odenbach, A. M. Menzel, and G. K. Auernhammer, **12**, 228, publisher: The Royal Society of Chemistry.
[14] F. Serra, U. Tkalec, and T. Lopez-Leon, Frontiers in Physics **8** (2020), 10.3389/fphy.2020.00373.
[15] J. Notbohm, A. Lesman, P. Rosakis, D. A. Tirrell, and G. Ravichandran, **12**, 20150320 (2015).
[16] X. Wang, J. Jiang, J. Chen, Z. Asilehan, W. Tang, C. Peng, and R. Zhang, **15**, 1655, publisher: Nature Publishing Group.
[17] R. H. Clayton, E. A. Zhuchkova, and A. V. Panfilov, **90**, 378 (2006).
[18] C. Chen, S. Liu, X.-q. Shi, H. Chaté, and Y. Wu, **542**, 210, publisher: Nature Publishing Group.
[19] Q. Li, C.-H. Sue, S. Basu, A. Shveyd, W. Zhang, G. Barin, L. Fang, A. Sarjeant, J. F. Stoddart, and O. M. Yaghi, Angewandte Chemie International Edition **49**, 6751 (2010).
[20] F. B. Fuller, Proceedings of the National Academy of Sciences of the United States of America **68**, 815 (1971).
[21] H. Shudo, P. Wiesener, E. Kolodzeiski, *et al.*, Nature Communications **16**, 1074 (2025).
[22] J. Nogami, D. Hashizume, Y. Nagashima, *et al.*, Nature Synthesis **2**, 888 (2023).
[23] L. Doyle, J. Hallinan, J. Bolduc, *et al.*, Nature **528**, 585 (2015).
[24] L. A. Doyle, B. Takushi, R. D. Kibler, *et al.*, Nature Communications **14**, 6746 (2023).
[25] M. Nakahara, *Geometry, topology and physics*, Graduate student series in physics (Hilger, Bristol, 1990).
[26] L. H. Kauffman, *Knots and Physics* (World Scientific Publishing Company, NJ, 1991).
[27] K. Reidemeister, Abhandlungen aus dem Mathematischen Seminar der Universität Hamburg **5**, 7 (1927).
[28] W. E. Clark, M. Saito, and L. Vendramin, Journal of Knot Theory and Its Ramifications **25**, 1650024 (2016), https://doi.org/10.1142/S0218216516500243.
[29] W. F. Pohl, Journal of Mathematics and Mechanics **17**, 975 (1968), accessed: 2025-05-02.
[30] C. K. Au and T. C. Woo, Computer-Aided Design and Applications **1**, 1 (2004).
[31] I. J. Tickle, C. Flensburg, P. Keller, W. Paciorek, A. Sharff, C. Vonrhein, and G. Bricogne, "STARANISO," `https://staraniso.globalphasing.org/cgi-bin/staraniso.cgi` (2016), cambridge, United Kingdom: Global Phasing Ltd.
[32] D. J. Thouless, M. Kohmoto, M. P. Nightingale, and M. den Nijs, Phys. Rev. Lett. **49**, 405 (1982).
[33] K. v. Klitzing, G. Dorda, and M. Pepper, Phys. Rev. Lett. **45**, 494 (1980).
[34] M. V. Berry, Proc. R. Soc. London, Ser A. **392**, 45 (1984).
[35] To understand the meaning of time-reversal symmetry, think about taking a motion picture and then running the motion picture backwards, does what we see change? The simplest example to think about broken time reversal symmetry is to invoke the magnetic field created by an electromagnet. If we run the motion picture backwards, current goes the opposite direction, and the field direction is reversed. Hence, a magnetic field is odd under time reversal symmetry.
[36] F. D. M. Haldane, Phys. Rev. Lett. **61**, 2015 (1988).
[37] While the integer quantum Hall effect is characterized by a $\mathbb{Z}$ topological invariant in two dimensions, a $\mathbb{Z}_2$ topological invariant was introduced by Kane and Mele to characterize the quantum spin Hall effect in systems with time-reversal symmetry. The $\mathbb{Z}_2$ index indicates the presence of a pair of helical edge states within the band gap around the system boundary, which are robust against time-reversal symmetry-preserving perturbations.
[38] M. P. Anantram and F. Léonard, Reports on Progress in Physics **69**, 507 (2006).
[39] R. Okuyama, W. Izumida, and M. Eto, Phys. Rev. B **99**, 115409 (2019).
[40] W. Izumida, R. Okuyama, A. Yamakage, and R. Saito, Phys. Rev. B **93**, 195442 (2016).
[41] S. Hu, M. Lundgren, and A. J. Niemi, Phys. Rev. E **83**, 061908 (2011).
[42] D. Goundaroulis, J. Dorier, F. Benedetti, and A. Stasiak, Scientific Reports **7**, 6309 (2017).
[43] K. Barkataki, L. H. Kauffman, and E. Panagiotou, Journal of Knot Theory and Its Ramifications **33**, 2450006 (2024), https://doi.org/10.1142/S0218216524500068.
[44] J. Janowski, V. A. B. Pham, S. Vecchioni, K. Woloszyn, B. Lu, Y. Zou, B. Erkalo, L. Perren, J. Rueb, J. Madnick, C. Mao, M. Saito, Y. P. Ohayon, N. Jonoska, and R. Sha, Proceedings of the National Academy of Sciences of the United States of America **121**, e2321992121 (2024).

https://doi.org/10.26434/chemrxiv-2025-swzkq **ORCID:** https://orcid.org/0000-0001-8243-650X Content not peer-reviewed by ChemRxiv. **License:** CC BY-NC-ND 4.0

[45] L. H. Kauffman, Topology **26**, 395 (1987).
[46] S. Grishanov, V. Meshkov, and A. Omelchenko, Textile Research Journal **79**, 702 (2009).
[47] S. Grishanov, V. Meshkov, and A. Omelchenko, Textile Research Journal **79**, 822 (2009).
[48] E. Kvavadze, O. Bar-Yosef, A. Belfer-Cohen, E. Boaretto, N. Jakeli, Z. Matskevich, and T. Meshveliani, Science **325**, 1359 (2009), https://www.science.org/doi/pdf/10.1126/science.1175404.
[49] V. F. R. Jones, Bulletin of the American Mathematical Society **12**, 103 (1985), mSC (1980): Primary 57M25; Secondary 46L10, MathSciNet: 766964.
[50] S. Grishanov, V. Meshkov, and A. Omelchenko, Textile Research Journal **79**, 702 (2009).
[51] S. Grishanov, V. Meshkov, and A. Omelchenko, Textile Research Journal **79**, 822 (2009).
[52] W. Zhou *et al.*, Science **387**, 269 (2025).
[53] S. Tawfick and I. Arretche, Science **387**, 250 (2025).
[54] E. Panagiotou, C. Tzoumanekas, S. Lambropoulou, K. C. Millett, and D. N. Theodorou, Progress of Theoretical Physics Supplement **191**, 172 (2011).
[55] E. Piskadlo and R. A. Oliveira, **18**, 2751 (2017).
[56] J. C. Wang, Journal of Molecular Biology **55**, 523 (1971).
[57] M. Gellert, K. Mizuuchi, M. H. O'Dea, and H. A. Nash, Proceedings of the National Academy of Sciences of the United States of America **73**, 3872 (1976).
[58] M. Vayssières *et al.*, Science **384**, 227 (2024).
[59] B. Connolly, C. A. Parsons, F. E. Benson, H. J. Dunderdale, G. J. Sharples, R. G. Lloyd, and S. C. West, Proceedings of the National Academy of Sciences of the United States of America **88**, 6063 (1991).
[60] N. C. Seeman, Journal of Theoretical Biology **99**, 237 (1982).
[61] N. Seeman and N. Kallenbach, Biophysical Journal **44**, 201 (1983).
[62] C. Mao, W. Sun, and N. C. Seeman, Journal of the American Chemical Society **121**, 5437 (1999).
[63] J. Chen and N. C. Seeman, Nature **350**, 631 (1991).
[64] E. Winfree, F. Liu, L. Wenzler, and N. C. Seeman, Nature **394**, 539 (1998).
[65] N. C. Seeman, Leonardo **47**, 142 (2014).
[66] D. Liu, G. Chen, U. Akhter, Z. Zhu, Y. Liu, D. Shu, P. Guo, and N. C. Seeman, Nature Chemistry **8**, 907 (2016).
[67] J. M. Simien and E. Haglund, Trends in Biochemical Sciences **46**, 461 (2021).
[68] T. Liu, X. Ma, J. Yu, W. Yang, G. Wang, Z. Wang, Y. Ge, J. Song, H. Han, W. Zhang, D. Yang, X. Liu, and M. Ma, Chem. Sci. **12**, 12353 (2021).
[69] A. R. Orun, C. K. Slaughter, E. T. Shields, A. Vajapayajula, S. Jones, R. Shrestha, and C. D. Snow, ACS Nanoscience Au **4**, 338 (2024).
[70] L. T. Glasby, J. L. Cordiner, J. C. Cole, and P. Z. Moghadam, Chemistry of Materials **36**, 9013 (2024).
[71] P. F. Faísca, Computational and Structural Biotechnology Journal **13**, 459 (2015).
[72] E. Panagiotou, Journal of Computational Physics **300**, 533 (2015).
[73] S. Wang, S. S. Park, C. T. Buru, *et al.*, Nature Communications **11**, 2495 (2020).
[74] H.-C. Z. Li, M. Eddaoudi, M. O'Keeffe, and O. M. Yaghi, Nature **402**, 276 (1999).
[75] V. Saranathan, S. Narayanan, A. Sandy, E. R. Dufresne, and R. O. Prum, Proceedings of the National Academy of Sciences of the United States of America **118**, e2101357118 (2021).
[76] N. Fujita and O. Terasaki, Phys. Rev. B **72**, 085459 (2005).
[77] V. Saranathan, C. O. Osuji, S. G. J. Mochrie, H. Noh, S. Narayanan, A. Sandy, E. R. Dufresne, and R. O. Prum, Proceedings of the National Academy of Sciences of the United States of America **107**, 11676 (2010).
[78] S. Ramachandran, K.-H. Ernst, G. D. Bachand, V. Vogel, and H. Hess, Small **2**, 330 (2006).
[79] N. S. Babcock, G. Montes-Cabrera, K. E. Oberhofer, M. Chergui, G. L. Celardo, and P. Kurian, The Journal of Physical Chemistry B **128**, 4035 (2024), published: 2024/05/02.
[80] P. S. Gurel, L. Y. Kim, P. V. Ruijgrok, T. Omabegho, Z. Bryant, and G. M. Alushin, eLife **6**, e31125 (2017).
[81] G. Lebreton, C. Géminard, F. Lapraz, S. Pyrpassopoulos, D. Cerezo, P. Spéder, E. M. Ostap, and S. Noselli, Science **362**, 949 (2018), https://www.science.org/doi/pdf/10.1126/science.aat8642.
[82] R. Süsstrunk and S. D. Huber, Science **349**, 47 (2015).
[83] R. B. Woodward and R. Hoffmann, Angewandte Chemie International Edition in English **8**, 781 (1969).
[84] T. Markussen, R. Stadler, and K. S. Thygesen, Nano Letters **10**, 4260 (2010).
[85] J. Gu, W. Wu, T. Stuyver, D. Danovich, R. Hoffmann, Y. Tsuji, and S. Shaik, Journal of the American Chemical Society **141**, 6030 (2019).
[86] B. Lu, S. Vecchioni, Y. P. Ohayon, J. W. Canary, and R. Sha, Biophysical Journal **121**, 4759 (2022).
[87] F. Zhang, C. R. Simmons, J. Gates, Y. Liu, and H. Yan, Angewandte Chemie International Edition **57**, 12504 (2018), https://onlinelibrary.wiley.com/doi/pdf/10.1002/anie.201807223.
[88] C. Zhang, J. Zhao, B. Lu, N. C. Seeman, R. Sha, N. Noinaj, and C. Mao, Journal of the American Chemical Society **145**, 4853 (2023).
[89] B. Lu, S. Vecchioni, Y. P. Ohayon, K. Woloszyn, T. Markus, C. Mao, N. C. Seeman, J. W. Canary, and R. Sha, Small **19**, 2205830 (2023), https://onlinelibrary.wiley.com/doi/pdf/10.1002/smll.202205830.
[90] G. Kolesov, P. Virnau, M. Kardar, and L. A. Mirny, Nucleic Acids Research **35**, W425 (2007).
[91] S. Misaghi, P. J. Galardy, W. J. Meester, H. Ovaa, H. L. Ploegh, and R. Gaudet, Journal of Biological Chemistry **280**, 1512 (2005).
[92] T. Sawada, A. Saito, K. Tamiya, K. Shimokawa, Y. Hisada, and M. Fujita, Nature Communications **10**, 921 (2019).
[93] D. Lyu, W. Xu, J. E. L. Payong, *et al.*, Nature Communications **13**, 3980 (2022).
[94] L. Wei, X. Hai, T. Xu, *et al.*, Nature Communications **15**, 2411 (2024).
[95] J. Teyssier, S. V. Saenko, D. van der Marel, and M. C. Milinkovitch, Nature Communications **6**, 6368 (2015).
[96] B. Alberts, A. Johnson, J. Lewis, M. Raff, K. Roberts, and P. Walter, *Molecular Biology of the Cell* (Garland Science, 2014).
[97] H. Hess and J. L. Ross, Chem. Soc. Rev. **46**, 5570 (2017).
[98] V. Subramanyan, K. L. Kirkpatrick, S. Vishveshwara, and S. Vishveshwara, Europhysics Letters **143**, 46001 (2023).
[99] A. Mentes, A. Huehn, X. Liu, A. Zwolak, R. Dominguez, H. Shuman, E. M. Ostap,

https://doi.org/10.26434/chemrxiv-2025-swzkq **ORCID:** https://orcid.org/0000-0001-8243-650X Content not peer-reviewed by ChemRxiv. **License:** CC BY-NC-ND 4.0

and C. V. Sindelar, Proceedings of the National Academy of Sciences **115**, 1292 (2018), https://www.pnas.org/doi/pdf/10.1073/pnas.1718316115.
[100] E. Prodan, K. Dobiszewski, A. Kanwal, J. Palmieri, and C. Prodan, Nature Communications **8**, 14587 (2017).
[101] D. Z. Manrique, C. Huang, M. Baghernejad, X. Zhao, O. A. Al-Owaedi, H. Sadeghi, V. Kaliginedi, W. Hong, M. Gulcur, T. Wandlowski, M. R. Bryce, and C. J. Lambert, Nature Communications **6**, 6389 (2015).
[102] K. Yoshizawa, Accounts of Chemical Research **45**, 1612 (2012).
[103] Y. Tsuji and R. Hoffmann, Angewandte Chemie International Edition **53**, 4093 (2014).
[104] G. C. Solomon, D. Q. Andrews, R. P. Van Duyne, and M. A. Ratner, The Journal of Chemical Physics **129**, 054701 (2008).
[105] D. Nozaki, H. Sevincli, S. M. Avdoshenko, R. Gutierrez, and G. Cuniberti, Phys. Chem. Chem. Phys. **15**, 13951 (2013).
[106] D. Nozaki, H. Sevincli, S. M. Avdoshenko, R. Gutierrez, and G. Cuniberti, Journal of Physics: Conference Series **427**, 012013 (2013).
[107] T. Stuyver, S. Fias, F. De Proft, and P. Geerlings, The Journal of Physical Chemistry C **119**, 26390 (2015).
[108] G. Posnjak, X. Yin, P. Butler, O. Bienek, M. Dass, S. Lee, I. D. Sharp, and T. Liedl, Science **384**, 781 (2024), https://www.science.org/doi/pdf/10.1126/science.adl2733.

https://doi.org/10.26434/chemrxiv-2025-swzkq **ORCID:** https://orcid.org/0000-0001-8243-650X Content not peer-reviewed by ChemRxiv. **License:** CC BY-NC-ND 4.0